A Journal of the Gesellschaft Deutscher Chemiker

Angewandte International Edition GDCh Chemie

www.angewandte.org

Accepted Article

Title: Light, Heat and Electricity Integrated Energy Conversion System: Photothermal-assisted Co-electrolysis of CO2 and Methanol

Authors: Yi-Rong Wang, Hui-Min Ding, Sheng-Nan Sun, Jing-Wen Shi, Yi-Lu Yang, Qi Li, Yifa Chen, Shun-Li Li, and Ya-Qian Lan

To be cited as: *Angew. Chem. Int. Ed.* **2022**, e202212162

Link to VoR: https://doi.org/10.1002/anie.202212162

WILEY-VCH

10.1002/anie.202212162

RESEARCH ARTICLE

WILEY-VCH

Light, Heat and Electricity Integrated Energy Conversion System: Photothermal-assisted Co-electrolysis of CO_2 and Methanol

Yi-Rong Wang[a]+, Hui-Min Ding[b]+, Sheng-Nan Sun[a], Jing-wen Shi[a], Yi-Lu Yang[a], Qi Li[a], Yifa Chen[a]*, Shun-Li Li[a] & Ya-Qian Lan[a]*

[a] Dr. Y.-R. W., S.-N. S., J.-W. S., Y.-L. Y., Q. L., Prof. Y. C., Prof. S.-L. L., and Prof. Y. -Q. L
School of Chemistry
South China Normal University
Guangzhou, 510006, P. R. China
E-mail: chyf927821@163.com; E-mail: yqlan@m.scnu.edu.cn;

[b] H.-M. D.
School of Chemistry and Materials Science
Nanjing Normal University
Nanjing 210023, P. R. China.

+These authors contributed equally to this work.

Supporting information for this article is given via a link at the end of the document.

Abstract: Strategy that can design powerful photothermal-catalysts to achieve photothermal-effect assisted coupling-catalysis is much desired for the improvement of energy conversion efficiency and redox product value in CO_2 electroreduction system. Herein, a kind of bifunctional viologen-containing covalent organic framework (Ni-2CBpy^{2+}-COF) has been prepared and successfully applied in photothermal-assisted co-electrolysis of CO_2 and methanol. Specifically, the FE_{CO} (cathode) and FE_{HCOOH} (anode) for Ni-2CBpy^{2+}-COF can reach up to ~100% at 1.9 V with ~31.5% saved overall electricity-consumption when the anodic oxygen evolution reaction (OER) is replaced by methanol oxidation. The superior performance could be attributed to the cyclic diquats in Ni-2CBpy^{2+}-COF that enhance the photothermal effect (ΔT = 49.1 °C) to accelerate faster charge transfer between catalyst and immediate species as well as higher selectivity towards desired products as revealed by DFT calculations and characterizations.

Introduction

CO_2 electrochemical reduction reaction (CO_2RR) enables the conversion of CO_2 into valuable chemicals or fuels by renewable electricity, which would simultaneously alleviate energy crisis and achieve global carbon balance.[1] However, the implementation of CO_2RR still needs to conquer considerable electricity consumption required by the sluggish kinetics of oxygen evolution reaction (OER) in the anode (~90% of the total energy), which would result in high energy consumption, low selectivity and overall energy conversion efficiency of the system.[2] Specifically, O_2, serving as the low value-added product of OER with a high standard molar Gibbs free energy of formation (237.1 kJ mol^{-1}), is generally responsible for the major energy loss of the system.[3] Therefore, it is highly desirable to find a thermodynamically flexible and kinetically favorable oxidation reaction to replace OER, aiming to improve the energy conversion efficiency of the CO_2RR system and generate high-value chemicals with lower energy consumption.[4] Typically, some organic molecules (e.g., methanol, 5-hydroxymethylfurfural, hydrazine, urea, glycerol, or primary amines) based oxidation reactions, possessing relatively lower anodic overpotential than OER, can serve as potential candidates to replace OER to achieve energy-saving electrolytic reaction systems.[5] In this regard, not only upgraded chemicals than O_2 but also decreased electricity consumption can be gained at anode, which enables to further enhance the anodic kinetics and overall energy conversion efficiency. Thus, it would be highly demanded to explore such powerful tandem systems to fulfill the unmet requirements of electrocatalytic CO_2RR.

Methanol, as an excellent energy vector in future electric cars industry, theoretically delivers 4 electrons per molecule at lower theoretical oxidation potential of 0.103 V than that of OER (1.23 V vs. RHE).[6] Additionally, methanol (~\$0.35 kg^{-1}) can be converted into the valuable chemicals like HCOOH (~\$1.08 kg^{-1}), which is advantageous by itself and can reduce the overall fuel cost.[4b, 6-7] In view of this, methanol oxidation reaction (MOR) coupling with CO_2RR might be a promising way to increase the overall electrocatalytic reaction rate and generate upgraded chemical HCOOH at the anode to replace OER.[8] In addition, when coupled with photon energy, the light irradiation would strongly influence the electronic property of light sensitive electrocatalysts, thus changing the activity and selectivity of co-electrolysis of CO_2 and methanol.[9] However, the exploration of this filed is still rare and limited by the lack of functional electrocatalysts that can meet the multi-requirements of such complex system. In this regard, it would be much essential to develop proper electrocatalysts for photothermal-assisted co-electrolysis of CO_2 and methanol with fast kinetics as well as high selectivity toward desired products.

Up to date, some nanomaterials (e.g., CuONS/CF or Ni_3C)[6, 7b, 8, 10] have been reported for typical co-electrolysis of CO_2 and methanol yet these explorations are still at an early stage with some unresolved issues, such as: 1) the reported Ru, Pd and Pt-based electrocatalysts for MOR with high activity are expensive with over-oxidation ability, which cannot selectively convert methanol to HCOOH and rare to empower the methanol economy; 2) two different types of catalysts are generally required for MOR and CO_2RR in most of reported co-electrolysis system, which would increase the cost and design difficulty of electrocatalysts and 3) these reported catalysts are mostly nanomaterials and usually lack clear structure models to understand the specific structure-property relationship or reaction mechanisms. Besides, photothermal-assisted techniques have been rarely reported to be applied in such co-

electrolysis system as far as we know. Therefore, the design of powerful and bifunctional electrocatalysts with well-defined structure and high activity/selectivity for photothermal-assisted co-electrolysis of CO_2 and methanol is largely demanded. Covalent organic framework (COF), holding specific properties like high stability, adjustable structure and accessible pore channel, has been regarded as ideal platforms for mass transport, substrate adsorption/activation and intermediate species transmission during the MOR and CO_2RR processes.[11] Especially attractive are their advantages in incorporation of functional organic units into COF frameworks, which can endow COFs with distinct photo/electro-redox activity for photothermal-assisted co-electrolysis of CO_2 and methanol. For example, metalloporphyrin unit, as a photosensitive aromatic macrocyclic conjugated π-electron system, holds efficient light absorption capability and electron mobility, has proven to be advantageous in CO_2RR.[12] Moreover, viologen derivative units, as a distinctive electron-transfer mediator, can generate photothermal effect and render prominent electron-transfer capability in photoelectric system to improve reaction kinetics and efficiency in redox catalytic systems.[13] In addition, COFs with these multifunctional groups that can be used for photothermal-assisted co-electrolysis of CO_2 and methanol have not received sufficient attention and reported yet. Thus, the specially designed COFs with bifunction will be ideal models as the electrode catalysts to realize simultaneous photothermal-assisted co-electrolysis of CO_2 and methanol.

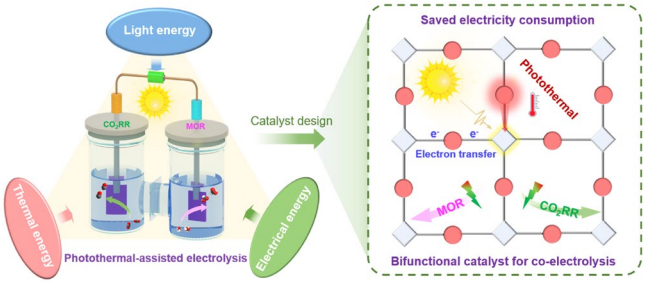

Scheme 1. The schematic illustration of photothermal-assisted co-electrolysis of CO_2 and methanol.

Herein, we have synthesized a kind of bifunctional viologen-containing COF (Ni-2CBpy^{2+}-COF) through the facile modification of Ni-Bpy-COF and applied it in photothermal-assisted co-electrolysis of CO_2 and methanol (Scheme 1). The cyclic diquats (2CBpy^{2+}) with viologen nature can serve as the electron-transfer mediator to accelerate the charge transfer between the catalyst and immediate species, which can generate strong photothermal effect (ΔT = 49.1 °C) for enhancing the whole reaction kinetics. Specifically, the FE_{CO} (cathode) and FE_{HCOOH} (anode) for Ni-2CBpy^{2+}-COF can reach up to ~100% at 1.9 V with ~31.5% saved overall electricity-consumption when the anodic OER is replaced by methanol electro-oxidation in the photothermal-assisted co-electrolysis system. Moreover, the vital role of Ni-2CBpy^{2+}-COF and the detailed catalytic mechanism are systematically investigated by various characterizations and DFT calculations. This work not only provides a new pathway to improve the systematic energy conversion efficiency of CO_2RR but also facilitate the potential practical applications of CO_2 electroreduction catalysts.

Results and Discussion

For the preparation of Ni-2CBpy^{2+}-COF, Ni-Bpy-COF is firstly synthesized by a solvothermal method via Schiff-base condensation between tetrakis(4-aminophenyl)-porphinato nickel (TAPP-Ni) and 2,2'-bipyridyl-5,5'-formaldehyde (Bpy).[14] Then, Ni-2CBpy^{2+}-COF is prepared by the reaction of Ni-Bpy-COF and dibromoethane at 120 °C in acetonitrile solvent for further characterizations (detail see Methods) (Figure 1a).[13a, 13b] According to the refined crystal structure, the Ni-Bpy-COF possesses one-dimensional channel, in which the adjacent two pyridine nitrogen in Bpy could be quaternized under reflux in acetonitrile forming ring closure as the reported study to generate the catalytic system.[13a, 13b] After quaternization, the powder X-ray diffraction (PXRD) pattern confirms that the synthesized Ni-2CBpy^{2+}-COF is similar to that of Ni-Bpy-COF, proving the well-remained crystallinity of Ni-2CBpy^{2+}-COF (Figure 1b). In addition, the quaternized Ni-2CBpy^{2+}-COF is further proved by the Fourier transform infrared (FT-IR) spectroscopy and X-ray photoelectron spectroscopy (XPS) tests (Figure 1c, S1 and S2). The FT-IR spectra of Ni-2CBpy^{2+}-COF show the new appeared stretches of methylene (-CH_2-) around 3000 cm^{-1} when compared with that of Ni-Bpy-COF, implying the ethylene group is part of the Ni-2CBpy^{2+}-COF framework (Figure 1c).[13a, 13b] Besides, the disappeared peak at 3315 cm^{-1} of N-H stretching vibration and a new peak appeared at 999 cm^{-1} of Ni-N stretching vibration when compared with TAPP confirm that the metal coordination occurred at the porphyrin center.[15] Meanwhile, the similar peaks at around 1620 cm^{-1} in Ni-Bpy-COF and Ni-2CBpy^{2+}-COF are ascribed to the C=N stretching vibration band, indicating the high stability during the quaternization process. The XPS results present that the Br 3d signal appearing at 67.6 eV in Ni-2CBpy^{2+}-COF is attributed to the bromide anion (Figure S1). In the N 1s spectrum, the binding energy at 399.2 eV and 398.5 eV are assigned to the imine and pyridine nitrogen, respectively.[13a, 13b] Compared with Ni-Bpy-COF, a new peak appeared at 402.0 eV for N 1s signal could be ascribed to the cyclic diquats in Ni-2CBpy^{2+}-COF, further proving the formation of quaternized BPy^{2+} moieties (Figure S1, S2).[13a, 13b] Moreover, the binding energy at 854.9 eV and 872.3 eV in Ni 2p spectrum are attributed to Ni (II) $2p_{3/2}$ and $2p_{1/2}$, respectively (Figure S1, S2).[16] Above the mentioned results indicate the successfully formation of Ni-2CBpy^{2+}-COF.

The nitrogen sorption measurement is performed at 77 K to characterize the structural porosity and specific surface area of Ni-Bpy-COF and Ni-2CBpy^{2+}-COF. Nitrogen adsorption-desorption curves show the existence of micropores for Ni-Bpy-COF and Ni-2CBpy^{2+}-COF (Figure S3). The Brunauer-Emmett-Teller surface area (S_{BET}) and total pore volume (V_t) of Ni-2CBpy^{2+}-COF are calculated to be 176 cm^2 g^{-1} and 0.09 cm^3 g^{-1}, respectively, which is lower than that of Ni-Bpy-COF (S_{BET}, 305 cm^2 g^{-1} and V_t, 0.21 cm^3 g^{-1}). Besides, the pore size distribution of Ni-Bpy^{2+}-COF is relatively broader and shifted to the micropore range of 1-2 nm with lower intensity than that of Ni-Bpy-COF, suggesting the presence of alkyl chains might partially occupy the pore channels after quaternization (Figure S3). In addition, CO_2 adsorption tests is carried out to analyze the CO_2

capture capability of Ni-Bpy-COF and Ni-2CBpy^{2+}-COF (Figure S4). Ni-2CBpy^{2+}-COF exhibits CO_2 uptake capacity of 30.5 cm^3 g^{-1}, 23.9 cm^3 g^{-1} and 19.6 cm^3 g^{-1} at 273 K, 283 K and 298 K, respectively, which is higher than that of Ni-Bpy-COF (26.5 cm^3 g^{-1}, 273 K; 19.8 cm^3 g^{-1}, 283 K and 17.4 cm^3 g^{-1}, 298 K) (Figure S4). The higher CO_2 adsorption of Ni-2CBpy^{2+}-COF than Ni-Bpy-COF indicates the cyclic diquats promotes the adsorption capacity of CO_2. Moreover, chemical stability of Ni-2CBpy^{2+}-COF is a vital parameter for further investigating its electrochemical performance. After immersing in 1 M KOH with 1 M methanol solution and 0.5 M $KHCO_3$ solution for more than 12 h, the PXRD patterns of the sample match well with that before treatment, confirming the well-remained crystalline structure and high chemical stability (Figure S5).

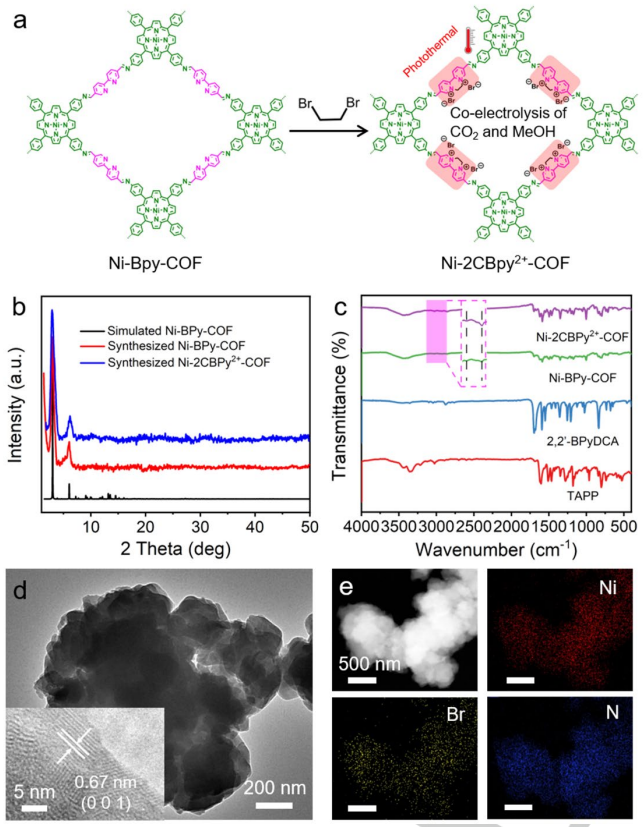

Figure 1. The preparation and characterization of Ni-Bpy-COF and Ni-2CBpy^{2+}-COF. (a) The scheme of the preparation of Ni-2CBpy^{2+}-COF. (b) The PXRD patterns of Ni-Bpy-COF and Ni-2CBpy^{2+}-COF. (c) The FT-IR spectra. (d) The HRTEM image of Ni-2CBpy^{2+}-COF. (e) STEM and mapping images of Ni-2CBpy^{2+}-COF.

The scanning electron microscopy (SEM) and transmission electron microscopy (TEM) images show that the Ni-Bpy-COF displays bulk morphology (Figure S6). After quaternization with dibromoethane, Ni-2CBpy^{2+}-COF remains the bulk morphology (Figure 1d, S7). The high-resolution transmission electron microscopy (HRTEM) image of Ni-2CBpy^{2+}-COF displays the oriented lattice fringes, in which the lattice spacing of 0.67 nm is ascribed to the (0 0 1) crystal facet of Ni-Bpy-COF, implying the high crystallinity of Ni-2CBpy^{2+}-COF (Figure 1d). Furthermore, the composition of the Ni-2CBpy^{2+}-COF is determined by scanning transmission electron microscopy (STEM) with an energy-dispersive X-ray spectrum (EDS), indicating that Ni, C, and N are uniformly distributed in Ni-2CBpy^{2+}-COF. (Figure 1e). The Ni element content in Ni-2CBpy^{2+}-COF is ~4.74 wt% as revealed by ICP-AES, which matches well with the result of EDS (Figure S8).

The electrocatalytic performances of the catalyst for CO_2RR, MOR and OER are conducted in H-type cell at selected potentials. The gas products can be monitored by gas chromatography (GC). The liquid products are detected and analyzed by ^{1}H nuclear magnetic resonance (^{1}H NMR) and ion chromatography (IC) test. The cathodic CO_2RR performance of catalyst is firstly investigated under the applied potential in 0.5 M $KHCO_3$. For comparison, linear sweep voltammetry (LSV) polarization curves are measured to evaluate the electrocatalytic activity of Ni-Bpy-COF and Ni-2CBpy^{2+}-COF. According to the LSV curves, Ni-Bpy-COF and 2CNi-Bpy^{2+}-COF show lower current density and larger onset potential in Ar saturated 0.5 M $KHCO_3$ solution than in CO_2 saturated 0.5 M $KHCO_3$ solution, illustrating the catalyst strongly favors CO_2RR than hydrogen evolution reaction (HER) (Figure S9). Additionally, Ni-2CBpy^{2+}-COF displays a higher total current density of -19.18 mA cm^{-2} at -1.1 V than Ni-Bpy-COF (-15.28 mA cm^{-2}), suggesting the excellent CO_2RR activity of 2CNi-Bpy^{2+}-COF (Figure 2a). To further estimate the selectivity of catalyst for CO_2RR, the Faradaic efficiency (FE) of the reduction product at different applied potentials is calculated from the quantitative results of GC and the sum of FE is found to be ~100% (Figure S10). The CO and H_2 are found to be the primary products and no liquid product has been detected by ^{1}H NMR (Figure 2b, S11). For Ni-2CBpy^{2+}-COF, the initial formation of CO is detected at overpotential of 290 mV. With the increase of potential, the FE_{CO} continuously increases and reaches up to a maximum value of ~98% at -0.9 V and keeps higher than 90% over a potential range from -0.8 to -1.0 V (Figure 2b). In contrast, the highest FE_{CO} of Ni-Bpy-COF is 94% at -1.0 V. Besides, the bare carbon paper and other additives (acetylene black (AB) and Nafion) are carried out as comparisons and no electrocatalytic CO_2RR activity are detected (Figure S12). The CO and H_2 partial current density at various potentials is calculated to indicate the remarkable catalytic activity of CO_2RR-to-CO over Ni-2CBpy^{2+}-COF. Ni-2CBpy^{2+}-COF gives a high partial CO current density of -14.6 mA cm^{-2} at -1.1 V, higher than that of Ni-Bpy-COF (-12.1 mA cm^{-2}) (Figure S13). These results indicate the superiority of Ni-2CBpy^{2+}-COF for CO_2RR.

Then, the anodic MOR performance of catalyst is measured. Initially, LSV curves of Ni-2CBpy^{2+}-COF are performed in 1 M KOH with different concentrations of methanol to optimize the concentration of methanol (Figure S14). The result shows that with the increase of methanol concentration, the anodic oxidation current density is gradually increasing. Thus, the concentration of methanol is optimized of 1 M in this work. Figure 2c presents the LSV curves of Ni-Bpy-COF and Ni-2CBpy^{2+}-COF for MOR and OER activity in 1 M KOH with and without 1 M methanol, respectively. As a result, the current density of Ni-2CBpy^{2+}-COF increases obviously in MOR and the anodic potential at current density of 10 mA cm^{-2} is 1.43 V, which is negatively shifted by 260 mV compared to that of OER (1.69 V). In comparison, for the Ni-Bpy-COF, the potential at current density of 10 mA cm^{-2} is 1.47 V for MOR, which is negatively shifted by 330 mV compared to that of OER. Besides, Tafel slope is a crucial parameter to represent the reaction

kinetics of MOR and OER (Figure S15). After calculation, the Tafel slope of Ni-2CBpy^{2+}-COF is calculated to be 56.8 mV dec^{-1} for MOR, which is much smaller than that of OER (189.5 mV dec^{-1}). These results imply that MOR is more conducive to occurring than OER. In addition, the FE of MOR is quantified by IC tests (Figure S16). The FE_{HCOOH} of Ni-2CBpy^{2+}-COF can reach up to a maximum value of ~92% at 1.4 V and keep higher than 85% over a wide potential range from 1.35 to 1.60 V (Figure 2d). In contrast, the highest FE_{HCOOH} of Ni-Bpy-COF is 74 % at 1.4 V. The bare carbon paper and other additives (AB and Nafion) are carried out as comparisons and no electrocatalytic MOR activity are detected (Figure S17). Moreover, the MOR partial current density of Ni-2CBpy^{2+}-COF (3.8 mA cm^{-2}) is higher than that of Ni-Bpy-COF (1.1 mA cm^{-2}) at 1.4 V (Figure S18). These results confirm the significant high activity and selectivity of Ni-2CBpy^{2+}-COF for MOR.

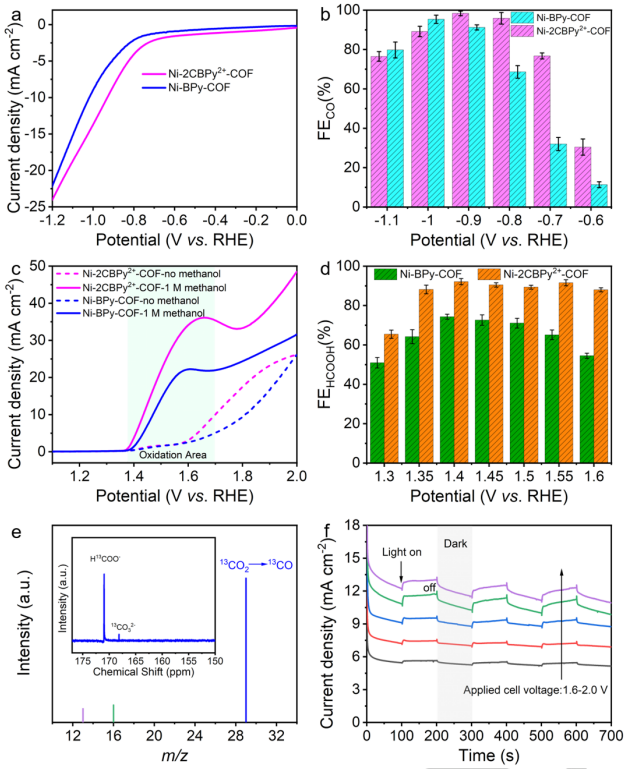

Figure 2. CO_2RR and MOR performance of Ni-Bpy-COF and Ni-2CBpy^{2+}-COF. (a) LSV curves of Ni-Bpy-COF and Ni-2CBpy^{2+}-COF at cathode in 0.5 M $KHCO_3$. (b) Faradaic efficiency for CO at different applied potentials of Ni-Bpy-COF and Ni-2CBpy^{2+}-COF (all reported values are average ones calculated from three or more independent measurements, and all errors are given as standard deviations). (c) LSV curves of Ni-Bpy-COF and Ni-2CBpy^{2+}-COF at anode in 1 M KOH with and without the addition of 1 M methanol. (d) Faradaic efficiency of MOR product at different applied potentials for Ni-Bpy-COF and Ni-2CBpy^{2+}-COF. (e) The mass spectra of ^{13}CO recorded under $^{13}CO_2$ atmosphere for CO_2RR and ^{13}C NMR spectrum of the electrolyte after MOR electrochemical test. (f) Photo-current response curves of Ni-2CBpy^{2+}-COF at different bias voltage.

To analyze the carbon source of the anodic oxidation and cathodic reduction products during the electrolysis, the isotopic-labeling experiment is conducted under identical reaction conditions (Figure 2e). For MOR, $^{13}CH_3OH$ is adopted as the substrate in the anodic electrolyte and the product is analyzed by ^{13}C NMR spectrum. The result shows that the peaks at about 171.1 ppm and 168.3 ppm are attributed to $HCOO^-$ and CO_3^{2-}, respectively (Figure 2e).[6] Besides, $^{13}CO_2$ is used as the substrate in CO_2RR process and the product is confirmed by gas chromatography mass spectra. As displayed in Figure 2e, the peak at m/z = 29 is ascribed to ^{13}CO. These evidences confirm that the carbon sources of oxidation and reduction products in MOR and CO_2RR indeed derive from the conversion of CH_3OH and CO_2.

Additionally, Nyquist plots based on electrochemical impedance spectroscopy (EIS) are recorded under the optimal potential to reveal the electrocatalytic kinetics on the electrode/electrolyte surface of sample during the electrolysis process (Figure S19). The Nyquist plots show distinct semicircles referring to the charge transfer resistance (Rct). The smaller semicircle gives a smaller value of Rct, suggesting the lower impedance and the faster efficient charge transfer between the interfaces. Apparently, the Rct for Ni-2CBpy^{2+}-COF in CO_2RR (20.72 Ω) and MOR (17.90 Ω) is much smaller than that of Ni-Bpy-COF (CO_2RR, 28.90 Ω; MOR, 45.08 Ω), implying that Ni-2CBpy^{2+}-COF is beneficial for the electron transfer process to enhance the catalytic reaction kinetics. Besides, the Rct for Ni-2CBpy^{2+}-COF in MOR (17.9 Ω) is smaller than that in OER (125.6 Ω), confirming a faster charge-transfer process for MOR. These results suggest that Ni-2CBpy^{2+}-COF could be utilized as efficient electrocatalyst for MOR and CO_2RR.

Motivated by the remarkable electrocatalytic performance for the anodic MOR and cathodic CO_2RR, Ni-2CBpy^{2+}-COF is used as bifunctional electrocatalyst for co-electrolysis of CO_2 and methanol that combines anodic MOR and cathodic CO_2RR (denoted as MOR||CO_2RR) in the two-electrode system to assess the feasibility of its practical application. As displayed in Figure S20, the LSV curves of Ni-2CBpy^{2+}-COF show that the MOR||CO_2RR required a lower cell voltage of 1.73 V to obtain the current density of 10 mA cm^{-2} than that for OER||CO_2RR (1.97 V), indicating the superiority of MOR||CO_2RR. To access the selectivity for MOR and CO_2RR in the two-electrode system, the products from the anode and cathode are separately collected and the FE values are calculated (Figure S21). Specifically, the FE_{CO} of Ni-2CBpy^{2+}-COF can retain higher than 75% over a wide cell voltage range from 1.8 to 2.0 V and reach up to the maximum value of 95% at 2 V, which is higher than that of OER||CO_2RR cell (FE_{CO} < 60%) (Figure S21). Meanwhile, the corresponding FE_{HCOOH} at anodic MOR is 94% at 1.9 V and higher than 75% at all applied cell voltages (Figure S21). In comparsion, the MOR||CO_2RR of Ni-Bpy-COF require a negative cell voltage (2.0 V) at the current density of 10 mA cm^{-2} compared to OER||CO_2RR (2.24 V) (Figure S22). The highest FE_{CO} and FE_{HCOOH} of Ni-Bpy-COF for MOR||CO_2RR is 74.4 % (2.0 V) and 78.7% (2.0 V), respectively, which is higher than that of OER||CO_2RR (FE_{CO} < 45.8%) (Figure S23, S24). Therefore, the co-electrolysis of CO_2 and methanol will generate the high value-added chemicals and improve the potential and economic feasibility of CO_2 utilization.

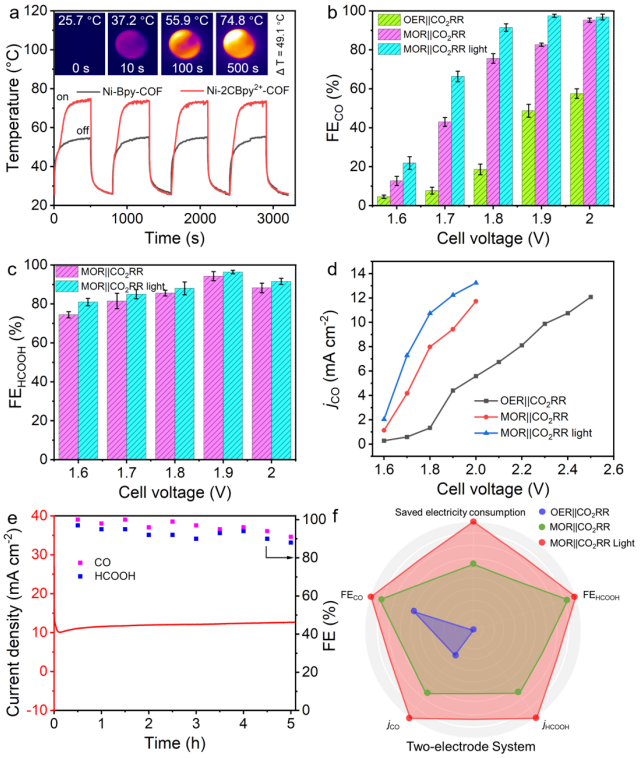

Figure 3. MOR||CO_2RR performance using Ni-2CBpy^{2+}-COF as anode and cathode catalyst. (a) Cycling tests of temperature changes of Ni-2CBpy^{2+}-COF and Ni-Bpy-COF under irradiation (insert images are the photothermal images of Ni-2CBpy^{2+}-COF). (b) The FE_{CO} (cathode) of OER||CO_2RR, MOR||CO_2RR and MOR||CO_2RR with light at different potentials using Ni-2CBpy^{2+}-COF as anode and cathode catalyst. (c) The FE_{HCOOH} (anode) of Ni-2CBpy^{2+}-COF for MOR||CO_2RR and MOR||CO_2RR with light at different potentials. (d) j_{CO} as a function of the cell voltage. (e) Long-term stability of Ni-2CBpy^{2+}-COF for MOR||CO_2RR with light irradiation at 1.9 V. (f) Radar chart of the performances for co-electrolysis of CO_2 and methanol in two-electrode system.

Ni-2CBpy^{2+}-COF with porphyrin and viologen derivative unit exhibits efficient light absorption capability, which will alter its electronic properties and eventually result in largely enhanced activity and energy efficiency (Figure S25).[17] Moreover, many previous reported works have illustrated that photo-assisted electrocatalysis is a promising way for CO_2 conversion into various value-added products.[9a, 9c, 12] In view of this, we proposed that light irradiation probably promote electrochemical activation of substrate molecule for co-electrolysis of CO_2 and methanol. To prove it, the photo-current test and photothermal conversion performance are conducted. Figure 2f shows that the current density increases obviously with the assistance of light, which provides a good test basis for the photothermal-assisted co-electrolysis of CO_2 and methanol. To evalute the photothermal conversion performance of Ni-2CBpy^{2+}-COF, the surface temperature of catalyst is monitored under light irradiation. As shown in the insert image of Figure 3a, the temperature differences (ΔT) before and after light irradiation for Ni-2CBpy^{2+}-COF is as high as 49.1 °C. In addition, the photothermal stability is studied by analyzing the "hot and cold" period of the catalyst (Figure 3a). The results show that the maximum temperature keeps nearly constant with the light on/off intervals. Then, the electrochemical performance of MOR||CO_2RR with light is conducted in the two-electrode system using Ni-2CBpy^{2+}-COF as anode and cathode catalyst. As displayed in Figure 3b and 3c, the FE_{CO} can maintain higher than 80% from 1.8 to 2.0 V cell voltage and even reach up to ~100% at 1.9 V, meanwhile, the corresponding FE_{HCOOH} keeep higher than 80% at all applied cell voltage (1.6 - 2.0 V) and reach the highest value of 97% at 1.9 V. The result indicates the MOR and CO_2RR performances under light irradiation are highly improved when compared with that of MOR||CO_2RR. In comparsion, the highest FE_{CO} and FE_{HCOOH} of Ni-Bpy-COF in MOR||CO_2RR under light irradiation are 78.8% and 81.7% at 2.0 V, respectively (Figure S26, S27). Electricity consumption is a vital factor to evaluate the energy conversion efficiency of the co-catalysis system. The electricity consumption is calculated depending on the j_{CO} value.[2e] The result displays that the electro-oxidation of methanol at the anode instead of the OER results in a 12.5 - 25% reduction in electricity requirement, thus improving the energy efficiency and process economic (Figure 3d). More importantly, by coupling with light, the anodic electro-oxidation of methanol can lower electricity consumption by up to 31.5% in the photothermal-assisted co-electrolysis of CO_2 and methanol system (Figure 3d).

The durability is a key factor for evaluating the practicability of catalysts. To access the stability of Ni-2CBpy^{2+}-COF in the two-electrode system, long-term test is recorded via chronoamperometric curves and monitoring variations in products at intervals (Figure 3e). After 5 h durability test at 1.9 V cell voltage, the current density of Ni-2CBpy^{2+}-COF is 12.65 mA cm^{-2}, meanwhile the high FE_{HCOOH} of 88% and FE_{CO} of 91% for Ni-2CBpy^{2+}-COF are still maintained, demonstrating that Ni-2CBpy^{2+}-COF has excellent electrocatalytic stability. In addition, the structural stability of Ni-2CBpy^{2+}-COF is characterized by PXRD and XPS tests. The PXRD patterns imply that the peaks of Ni-2CBpy^{2+}-COF after the electrochemical test are consistent with that before the test (Figure S28). The XPS tests show that the Ni species has no obvious change after electrocatalytic test (Figure S29). The above results imply that Ni-2CBpy^{2+}-COF is a bifunctional electrocatalyst with high durability, which has much potential to be used in efficient photothermal-assisted co-electrolysis of CO_2 and methanol (Figure 3f).

In-situ ATR-FTIR studies are recorded to gain insight into the intermediates during the MOR and CO_2RR processes for further investigation of the reaction mechanism (Figure 4a, 4b). As displayed in Figure 4a, for MOR, the peak at 1473 cm^{-1} can be assigned to CH_2O*, which is the vital intermediate for the formation of HCOOH.[7b, 8, 18] Most importantly, the signals appeared at 1269 cm^{-1}, 1335 cm^{-1}, 1407 cm^{-1}, 1573 cm^{-1} and 1642 cm^{-1} are ascribed to the OH deformation, C-O stretch, symmetric stretch, asymmetric stretch and C=O stretch of *HCOOH, respectively.[18b] Moreover, in the spectra of CO_2RR (Figure 4b), the peaks detected at 1700 - 1200 cm^{-1} are assigned to the crucial intermediate (i.e. COOH*) for CO_2RR to CO.[19] Additionally, the band of chemisorbed CO (*CO) is appeared at 2050 cm^{-1} (Figure 4b). The detected vital intermediates set solid basis for further theoretical study to investigate the relative reaction mechanisms.

Density functional theory (DFT) calculations relating to work function of catalyst, and the free energy of CO_2RR and MOR are performed to reveal the catalytic mechanism (Figure S30). The work function describes the energy requirements for adding or removing an electron from a solid, which can be used to describe electron transfer on an electrode.[20] A lower work function value of an electrocatalyst corresponds to a higher

tunneling probability of electrons, which means that electrons are more easily transferred from the electrode to the reactant to participate in the reaction. The work function of Ni-Bpy-COF and Ni-2CBpy^{2+}-COF is given in Figure 4c. Specifically, Ni-2CBpy^{2+}-COF exhibits a lower work function (3.38 eV) when compared to Ni-Bpy-COF (3.47 eV), indicating the superior electronic properties of Ni-2CBpy^{2+}-COF in electron transferring that can result in largely enhanced activity and selectivity for photothermal-assisted co-electrolysis of CO_2 and methanol.

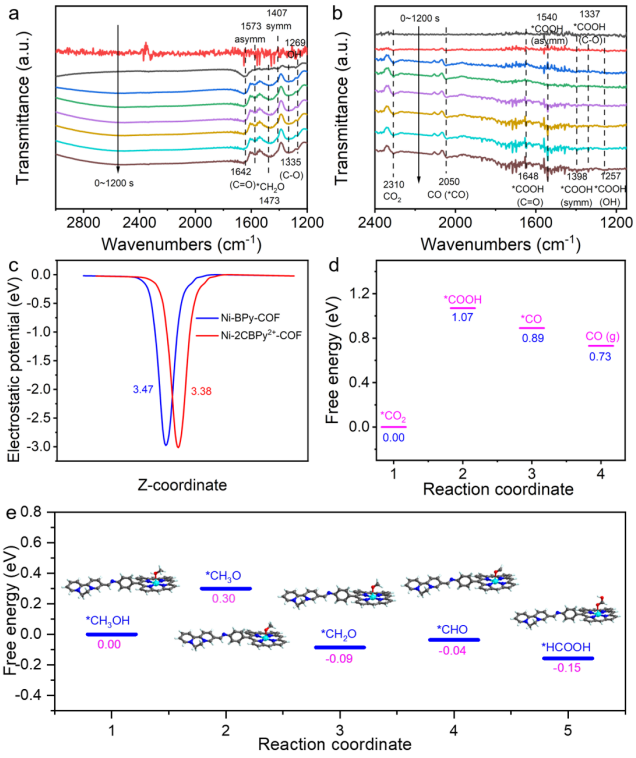

Figure 4. In-situ FTIR spectra of Ni-2CBpy^{2+}-COF for electrocatalysis and DFT calculations. (a) In-situ FTIR spectra of Ni-2CBpy^{2+}-COF for MOR. (b) In-situ FTIR spectra of Ni-2CBpy^{2+}-COF for CO_2RR. (c) Work function of Ni-2CBpy^{2+}-COF and Ni-Bpy-COF. (d) Free energy profiles of Ni-2CBpy^{2+}-COF for CO_2RR. (e) Free energy profiles of Ni-2CBpy^{2+}-COF for MOR. Insert image: structures of the reaction intermediates involved in the proposed reaction mechanism for the MOR-to-HCOOH on Ni-2CBpy^{2+}-COF catalyst.

After revealing the difference in activity and selectivity, DFT calculations are subsequently studied to reveal the detailed free energy diagram for each reaction coordinate during CO_2RR and MOR pathways on Ni-2CBpy^{2+}-COF. Generally, the electroreduction of CO_2 to CO involves three elementary reactions, the formation of *COOH and *CO with one (H^+/e^-) pair transfer for each of them, and the finally CO desorption process.[21] From the free energy diagram displayed in Figure 4d, the rate-determining step for CO_2RR on Ni-2CBpy^{2+}-COF is the formation of adsorbed intermediates *COOH with high free energy of ΔG = 1.07 eV. In addition, the specific MOR-to-HCOOH reaction pathway (*CH_3OH → *CH_3O → *CH_2O → *CHO → *HCOOH, * represents the catalytic site) involves the oxidation of MeOH along with (H^+/e^-) pairs.[8] As displayed in Figure 4e, there are two nonspontaneous reaction steps with ΔG > 0 in the whole reaction pathway, including *CH_3OH → *CH_3O and *CH_2O → *CHO, in which the formation of *CH_3O with the largest free energy of ΔG = 0.30 eV is the rate-determining step. Then, the *CH_2O, *CHO and *HCOOH intermediates generate in turn involving the deep oxidation of CH_3OH along with (H^+/e^-) pairs. Finally, the produced HCOOH is quickly desorbed from the catalyst surface and efficiently transferred into electrolyte to finish the catalysis process.

Conclusion

In summary, a kind of viologen-containing covalent-organic-framework (Ni-2CBpy^{2+}-COF) has been synthesized and successfully applied in photothermal-assisted co-electrolysis of CO_2 and methanol as bifunctional electrocatalyst to simultaneous generate high-valued chemicals on the both electrode sides. Specifically, the cyclic diquats (2CBpy^{2+}) can serve as the electron-transfer mediator to accelerate the charge transfer between the catalyst and immediate species, and generate strong photothermal effect (ΔT = 49.1 °C) for enhancing the whole reaction kinetics as well as high selectivity toward desired products. Notably, the FE_{CO} (cathode) and FE_{HCOOH} (anode) for Ni-2CBpy^{2+}-COF can reach up to ~100% at 1.9 V with ~31.5% saved overall electricity-consumption when the anodic OER is replaced by methanol electro-oxidation in the photothermal-assisted co-electrolysis system. Moreover, the vital role of Ni-2CBpy^{2+}-COF and the detailed catalytic mechanism are systematically investigated by various *in/ex-situ* characterizations and DFT calculations. This work opens great perspective for the systematic design of CO_2RR coupling with organic molecule oxidation reaction in improving the total energy conversion efficiency and generation of value-added chemicals, which might contribute to the practical application process of electrocatalytic CO_2RR.

Supplemental Information includes 30 figures

Acknowledgements

This work was financially supported by the National Natural Science Foundation of China (Grants 21871141, 21871142, 22071109, 21901122, 22225109 and 22171139), Postdoctoral Innovation Talent Support Program (BX20220116).

Conflict of Interest

The authors declare no conflict of interest.

Keywords: Co-electrolysis of CO_2 and Methanol • Photothermal conversion effect • Photothermal-assisted • Bifunctional catalysts

References

[1] a) Y. Li, A. Ozden, W. R. Leow, P. Ou, J. E. Huang, Y. Wang, K. Bertens, Y. Xu, Y. Liu, C. Roy, H. Jiang, D. Sinton, C. Li, E. H. Sargent, *Nat. Catal.* **2022**, *5*, 185-192; b) X. Chen, J. Chen, N. M. Alghoraibi, D. A. Henckel, R. Zhang, U. O. Nwabara, K. E. Madsen, P. J. A. Kenis, S. C. Zimmerman, A. A. Gewirth, *Nat. Catal.* **2021**, *4*, 20-27; c) E. Huang Jianan, F. Li, A. Ozden, A. Sedighian Rasouli, F. P. García de Arquer, S. Liu, S. Zhang, M. Luo, X. Wang, Y. Lum, Y. Xu, K. Bertens, K. Miao Rui, C.-T.

Dinh, D. Sinton, H. Sargent Edward, *Science* **2021**, *372*, 1074-1078; d) Y.-R. Wang, H.-M. Ding, X.-Y. Ma, M. Liu, Y.-L. Yang, Y. Chen, S.-L. Li, Y.-Q. Lan, *Angew. Chem. Int. Ed.* **2022**, *61*, e202114648.

[2] a) Z. Gu, H. Shen, Z. Chen, Y. Yang, C. Yang, Y. Ji, Y. Wang, C. Zhu, J. Liu, J. Li, T.-K. Sham, X. Xu, G. Zheng, *Joule* **2021**, *5*, 429-440; b) C. Cao, D.-D. Ma, J. Jia, Q. Xu, X.-T. Wu, Q.-L. Zhu, *Adv. Mater.* **2021**, *33*, 2008631; c) X. Tan, C. Yu, Y. Ren, S. Cui, W. Li, J. Qiu, *Energy Environ. Sci.* **2021**, *14*, 765-780; d) L. Fan, Y. Ji, G. Wang, J. Chen, K. Chen, X. Liu, Z. Wen, *J. Am. Chem. Soc.* **2022**, *144*, 7224-7235; e) S. Verma, S. Lu, P. J. A. Kenis, *Nat. Energy* **2019**, *4*, 466-474.

[3] a) Y. Xu, B. Zhang, *ChemElectroChem* **2019**, *6*, 3214-3226; b) Q. Zhou, Z. Shen, C. Zhu, J. Li, Z. Ding, P. Wang, F. Pan, Z. Zhang, H. Ma, S. Wang, H. Zhang, *Adv. Mater.* **2018**, *30*, 1800140.

[4] a) R. Li, K. Xiang, Z. Peng, Y. Zou, S. Wang, *Adv. Energy Mater.* **2021**, *11*, 2102292; b) J. Na, B. Seo, J. Kim, C. W. Lee, H. Lee, Y. J. Hwang, B. K. Min, D. K. Lee, H.-S. Oh, U. Lee, *Nat. Commun.* **2019**, *10*, 5193.

[5] a) E. Pérez-Gallent, S. Turk, R. Latsuzbaia, R. Bhardwaj, A. Anastasopol, F. Sastre-Calabuig, A. C. Garcia, E. Giling, E. Goetheer, *Ind. Eng. Chem. Res.* **2019**, *58*, 6195-6202; b) X. Deng, M. Li, Y. Fan, L. Wang, X.-Z. Fu, J.-L. Luo, *Applied Catalysis B: Environmental* **2020**, *278*, 119339; c) M. S. E. Houache, R. Safari, U. O. Nwabara, T. Rafaïdeen, G. A. Botton, P. J. A. Kenis, S. Baranton, C. Coutanceau, E. A. Baranova, *ACS Applied Energy Materials* **2020**, *3*, 8725-8738; d) Y. Sun, X. Li, M. Yang, W. Xu, J. Xie, M. Ding, *Green Chem.* **2020**, *22*, 7543-7551; e) J.-Y. Zhang, H. Wang, Y. Tian, Y. Yan, Q. Xue, T. He, H. Liu, C. Wang, Y. Chen, B. Y. Xia, *Angew. Chem. Int. Ed.* **2018**, *57*, 7649-7653; f) Y. Huang, X. Chong, C. Liu, Y. Liang, B. Zhang, *Angew. Chem. Int. Ed.* **2018**, *57*, 13163-13166; g) Y. Lu, T. Liu, C.-L. Dong, C. Yang, L. Zhou, Y.-C. Huang, Y. Li, B. Zhou, Y. Zou, S. Wang, *Adv. Mater.* **2022**, *34*, 2107185; h) Y. Zhu, J. Zhang, Q. Qian, Y. Li, Z. Li, Y. Liu, C. Xiao, G. Zhang, Y. Xie, *Angew. Chem. Int. Ed.* **2022**, *61*, e202113082; i) W. Wang, Y.-B. Zhu, Q. Wen, Y. Wang, J. Xia, C. Li, M.-W. Chen, Y. Liu, H. Li, H.-A. Wu, T. Zhai, *Adv. Mater.* **2019**, *31*, 1900528.

[6] X. Wei, Y. Li, L. Chen, J. Shi, *Angew. Chem. Int. Ed.* **2021**, *60*, 3148-3155.

[7] a) D. Bellotti, L. Cassettari, M. Mosca, L. Magistri, *Journal of Cleaner Production* **2019**, *240*, 117947; b) J. Li, R. Wei, X. Wang, Y. Zuo, X. Han, J. Arbiol, J. Llorca, Y. Yang, A. Cabot, C. Cui, *Angew. Chem. Int. Ed.* **2020**, *59*, 20826-20830.

[8] J. Hao, J. Liu, D. Wu, M. Chen, Y. Liang, Q. Wang, L. Wang, X.-Z. Fu, J.-L. Luo, *Applied Catalysis B: Environmental* **2021**, *281*, 119510.

[9] a) V. Kumaravel, J. Bartlett, S. C. Pillai, *ACS Energy Lett.* **2020**, *5*, 486-519; b) X. Huang, Q. Shen, J. Liu, N. Yang, G. Zhao, *Energy Environ. Sci.* **2016**, *9*, 3161-3171; c) X. Deng, R. Li, S. Wu, L. Wang, J. Hu, J. Ma, W. Jiang, N. Zhang, X. Zheng, C. Gao, L. Wang, Q. Zhang, J. Zhu, Y. Xiong, *J. Am. Chem. Soc.* **2019**, *141*, 10924-10929.

[10] a) T.-J. Wang, F.-M. Li, H. Huang, S.-W. Yin, P. Chen, P.-J. Jin, Y. Chen, *Adv. Funct. Mater.* **2020**, *30*, 2000534; b) W. Huang, H. Wang, J. Zhou, J. Wang, P. N. Duchesne, D. Muir, P. Zhang, N. Han, F. Zhao, M. Zeng, J. Zhong, C. Jin, Y. Li, S.-T. Lee, H. Dai, *Nat. Commun.* **2015**, *6*, 10035; c) Q. Zhang, F. Yue, L. Xu, C. Yao, R. D. Priestley, S. Hou, *Applied Catalysis B: Environmental* **2019**, *257*, 117886; d) W. Gong, Z. Jiang, R. Wu, Y. Liu, L. Huang, N. Hu, P. Tsiakaras, P. K. Shen, *Applied Catalysis B: Environmental* **2019**, *246*, 277-283.

[11] a) H. S. Sasmal, A. Kumar Mahato, P. Majumder, R. Banerjee, *J. Am. Chem. Soc.* **2022**, *144*, 11482-11498; b) M. Lu, M. Zhang, J. Liu, Y. Chen, J.-P. Liao, M.-Y. Yang, Y.-P. Cai, S.-L. Li, Y.-Q. Lan, *Angew. Chem. Int. Ed.* **2022**, *61*, e202200003.

[12] a) D. Yang, H. Yu, T. He, S. Zuo, X. Liu, H. Yang, B. Ni, H. Li, L. Gu, D. Wang, X. Wang, *Nat. Commun.* **2019**, *10*, 3844; b) M. Lu, M. Zhang, C.-G. Liu, J. Liu, L.-J. Shang, M. Wang, J.-N. Chang, S.-L. Li, Y.-Q. Lan, *Angew. Chem. Int. Ed.* **2021**, *60*, 4864-4871.

[13] a) Z. Mi, T. Zhou, W. Weng, J. Unruangsri, K. Hu, W. Yang, C. Wang, K. A. I. Zhang, J. Guo, *Angew. Chem. Int. Ed.* **2021**, *60*, 9642-9649; b) Z. Mi, P. Yang, R. Wang, J. Unruangsri, W. Yang, C. Wang, J. Guo, *J. Am. Chem. Soc.* **2019**, *141*, 14433-14442; c) W. Ma, L. Xu, S. Zhang, G. Li, T. Ma, B. Rao, M. Zhang, G. He, *J. Am. Chem. Soc.* **2021**, *143*, 1590-1597.

[14] X. Chen, J. Gao, D. Jiang, *Chem. Lett.* **2015**, *44*, 1257-1259.

[15] Y.-R. Wang, M. Liu, G.-K. Gao, Y.-L. Yang, R.-X. Yang, H.-M. Ding, Y. Chen, S.-L. Li, Y.-Q. Lan, *Angew. Chem. Int. Ed.* **2021**, *60*, 21952-21958.

[16] S.-N. Sun, L.-Z. Dong, J.-R. Li, J.-W. Shi, J. Liu, Y.-R. Wang, Q. Huang, Y.-Q. Lan, *Angew. Chem. Int. Ed.* **2022**, *61*, e202207282.

[17] Q. Huang, J. Liu, L. Feng, Q. Wang, W. Guan, L.-Z. Dong, L. Zhang, L.-K. Yan, Y.-Q. Lan, H.-C. Zhou, *National Science Review* **2020**, *7*, 53-63.

[18] a) J.-D. Yi, R. Xie, Z.-L. Xie, G.-L. Chai, T.-F. Liu, R.-P. Chen, Y.-B. Huang, R. Cao, *Angew. Chem. Int. Ed.* **2020**, *59*, 23641-23648; b) X. Wang, S. Xi, W. S. V. Lee, P. Huang, P. Cui, L. Zhao, W. Hao, X. Zhao, Z. Wang, H. Wu, H. Wang, C. Diao, A. Borgna, Y. Du, Z. G. Yu, S. Pennycook, J. Xue, *Nat. Commun.* **2020**, *11*, 4647.

[19] N. J. Firet, W. A. Smith, *ACS Catal.* **2017**, *7*, 606-612.

[20] Z.-Z. Wu, F.-Y. Gao, M.-R. Gao, *Energy Environ. Sci.* **2021**, *14*, 1121-1139.

[21] Y.-R. Wang, Q. Huang, C.-T. He, Y. Chen, J. Liu, F.-C. Shen, Y.-Q. Lan, *Nat. Commun.* **2018**, *9*, 4466.

10.1002/anie.202212162

Entry for the Table of Contents

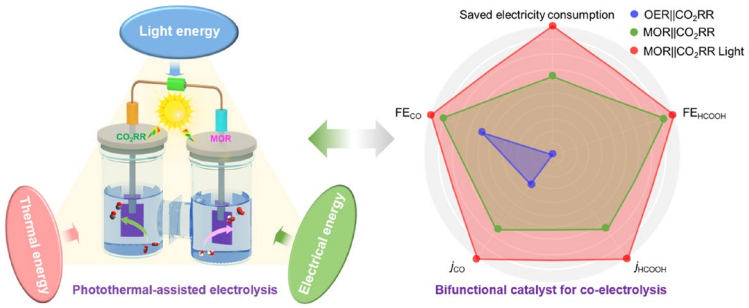

A kind of bifunctional viologen-containing covalent-organic-framework has been prepared and successfully applied in photothermal-assisted co-electrolysis of CO_2 and methanol. The superior performance could be attributed to the cyclic diquats in Ni-2CBpy^{2+}-COF that enhance the photothermal effect to accelerate faster charge-transfer between catalyst and immediate species as well as higher selectivity towards desired products.